TECHNICAL DESIGN REPORT

TEAM WingingIt - #30

Luciana Jaalouk – Team Captain
Juhi Singh
Marc Rozman
Eduardo Hernandez
Justin Talevski
Shivam Suleria

TABLE OF CONTENTS

1. OVERVIEW 2

1.1 ABOUT NYU 2
1.2 DISCRIMINATORS/INNOVATIONS 2

2. EXECUTIVE SUMMARY 2
3. SCHEDULE SUMMARY 3
4. DESIGN LAYOUT AND TRADES 3

4.1 WINGS 4
4.1.1 Airfoil 4
4.1.2 Wing Planform 5
4.1.3 Chord Length and Mean Aerodynamic Chord 5
4.1.4 Aspect Ratio, Surface Area and Mean Standard Chord Length 5
4.1.5 Wing Tips 6
4.2 FUSELAGE 6
4.3 TAIL 6
4.3.1 Horizontal Stabilizer 6
4.3.2 Vertical stabilizer 7
4.4 CONTROL SURFACE SIZING 7
4.5 LANDING GEAR 8
4.5.1 Configuration Selection 8
4.5.2 Layout Design and Wheel Size 8

5. ELECTRONICS 9

5.1 BATTERY 9
5.2 SPEED CONTROLLER AND WIRING 9
5.3 SERVOS 10
5.4 RADIO SYSTEM 10

6. POWER AND PROPULSION 10

6.1 MOTOR 10
6.2 PROPELLER 11
6.3 THRUST 11

7. LOADS 13
8. FLIGHT ANALYSIS AND AIRCRAFT PERFORMANCE 13

8.1 LIFT AND DRAG ANALYSIS 13
8.1.1 Lift on Airfoil and Wing 13
8.1.2 Drag Analysis 15
8.1.3 Full Model CFD Simulation 16
8.2 GROUND RUN AND TAKEOFF 16
8.3 MASS PROPERTIES AND BALANCE ..... ERROR! BOOKMARK NOT DEFINED.
8.4 PAYLOAD PREDICTION CURVE 17
8.5 STRUCTURAL ANALYSIS ..... ERROR! BOOKMARK NOT DEFINED.

9. STABILITY AND CONTROL 18

9.1 STATIC STABILITY 18
9.2 WEIGHT BALANCING AND BALLAST 20

10. MANUFACTURING 20

10.1 WINGS AND EMPENNAGE 20
10.2 FUSELAGE 21
10.3 ELECTRONICS 21
10.4 LANDING GEAR 21
10.5 ASSEMBLY 22

11. CONCLUSION 23
12. REFERENCES 24
APPENDIX A – LIST OF SYMBOLS AND ABBREVIATIONS 26

APPENDIX B – TECHNICAL DATA SHEET: PAYLOAD PREDICTION 27
APPENDIX C – 2D DRAWING 28

1. OVERVIEW

1.1 About NYU

Over the past decade, Mechanical and Aerospace Engineering students from New York University (NYU) have teamed up to compete in the Society of Automotive Engineers' (SAE) Aero Design Series. NYU has traditionally done admirably well, even placing first overall in 2011 under the Advanced Class. This year, the 2018 NYU SAE Aero Design team, WingingIt, plans on maintaining the legacy and achieving a formidable rank within the Regular Class.

1.2 Discriminators/Innovations

A study of previous aircrafts enabled the team to compile their successes and apply them to this year's design. The team chose to design large and thick wings with mixed taper in order to maximize the aspect ratio, lift and wetted area. The tapered section of the wing encompasses the ailerons. The fuselage has a unique cross-section, combining the benefits of a circular (aerodynamic) and rectangular (easy to manufacture) cross-section. The upper half is a rectangle for easy access to the cargo and passenger bays as well as wing attachment. The bottom portion is a nonagon which mimics a circular cross section, keeping mindful of manufacturing and assembly.

2. EXECUTIVE SUMMARY

The fuselage is 93.5 *in* long with taper in both front and back. The wings have a span of 141 *in*. The wings are tapered for about half of the length and have a NACA 6415 airfoil. The weight of the fully loaded aircraft containing 30 passengers is 51 *lb*. The maximum static thrust generated by the propeller is 11 *lb*. With such setup and no penalties, the team is expected to achieve a score of 93.75 points in the flight portion of the competition.

3. SCHEDULE SUMMARY

The team's formation commenced in early September and each member's roles and responsibilities were assigned. Brainstorming and research was conducted to formulate an optimal design. Basic hand calculations solidified initial ideas and designs, serving as sanity check. 3D CAD models were build and simulated in ANSYS. The initial aircraft design was finalized in November but was continuously updated as new considerations were brought about. The materials were procured by the end of January. Manufacturing began in January and was finished by mid-February. Mechanical and Electrical tests were conducted in February. A flight test was scheduled for mid-March to ensure the airworthiness of the aircraft before it is shipped out for the competition. Below is a table of the major deliverables.

Table 1: Schedule of Major Deliverables

Major Deliverable	Date (mm/dd/yyyy)
Airfoil Determinations	09/30/2017
Initial CAD Models	10/20/2017
Initial Simulations	10/31/2017
Revised CAD Models	11/20/2017
Final Simulations and CAD Revisions	12/30/2017
Final procurement of materials	01/30/2018
Wing and Empennage Fabrication	01/25/2018
Fuselage Fabrication	02/05/2018
Mechanical and Electrical Testing	02/15/2018
Test Flight	03/10/2018

4. DESIGN LAYOUT AND TRADES

The flowchart below provides a brief overview of the research process and trade-offs.

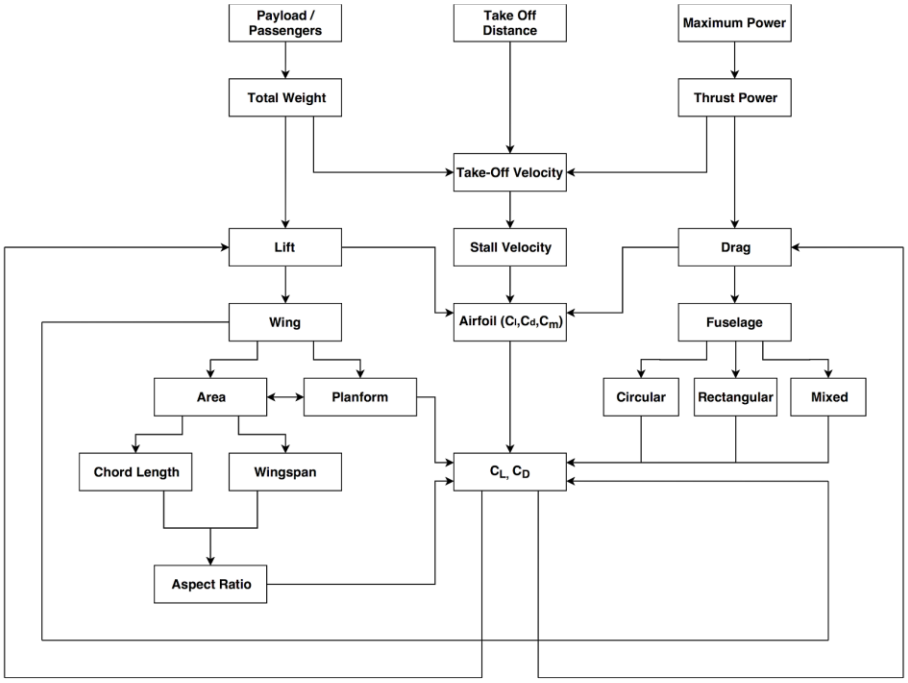

Figure 1: Design Process Flowchart

4.1 Wings

The wings are the most important component of an aircraft since they generate almost all the lift. The wings also contribute towards most of the drag in the form of both viscid and inviscid drag. For the team's design, the wing leading edge was placed 18 *in* away from the front of fuselage. A high wing design relative to the fuselage was chosen because it increases lateral stability since a lower center of gravity relative to the wings helps produce a keel effect, laterally stabilizing the aircraft after a disturbance.

4.1.1 Airfoil

4-series NACA airfoils are were widely used in propeller driven aircrafts. Since the team's aircraft is also, propeller driven, several NACA airfoils were simulated in the CFD package Fluent. A preliminary pool of airfoils was narrowed down to four promising airfoils based on lift and drag plots. The airfoils were tested for optimum camber, the position of the maximum camber and the thickness of the airfoil. MATLAB was used to generate the geometry of airfoils. Eventually, the NACA 6415 was selected as it provides high values of lift coefficients at low AoA and has a thick cross-section that increases mechanical strength.

4.1.2 Wing Planform

The elliptical wing planform has optimal pressure distribution over the wing, resulting in minimal loss of lift over the span. However, such a shape is difficult to manufacture. An easier way to produce a similar effect is by using a wing with taper. A combination of rectangular and tapered shape with a straight leading edge was used. For the first 37.5 *in*, the wing is rectangular. After that, the wing starts tapering while maintaining straight leading edge. The taper ratio is 0.7 and the tapered section spans 33 *in* on each side. The combination also helped in retaining a higher surface area.

Three different wing planforms were simulated: fully rectangular, fully tapered (λ= 0.7) and mixed taper (described above). The distribution of pressure over the wing surface was estimated from simulations. The results were interpreted in terms of lift generated. The planform that showed minimum change in pressure when following wingspan was selected. Figure 2 shows the contour plot of static pressure on the surface of the wing for the selected planform. It is observed that for most of the span, the static pressure is constant. Closer to the tip, the static pressure becomes less negative. Hence, less lift is generated at the tip. This is primarily due to the vortices. The Oswald efficiency factor, *e*, of such planform is assumed to be 0.85.

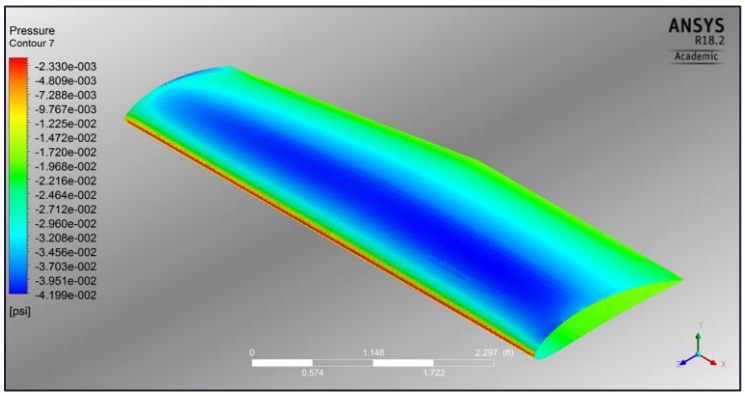

Figure 2: Pressure Distribution Over the Wing

4.1.3 Chord Length and Mean Aerodynamic Chord

The chord length of the root airfoil was decided to be 24 *in* for achieving high surface area. Since the input power is limited, a slow speed flight was expected. Therefore, to maximize lift, surface area was increased by increasing chord length. The mean aerodynamic chord was calculated to be 22.55 *in*. The tip airfoil chord length is 16.8 *in*. The thickness of airfoil is 15% of the chord length.

4.1.4 Aspect Ratio, Surface Area and Mean Standard Chord Length

The overall surface area of the wing was calculated to be 21.85 ft^2. The corresponding Aspect Ratio (AR) becomes 6.32. It is not surprising since the wingspan is limited. The corresponding mean standard chord length becomes 22.31 *in*.

4.1.5 Wing Tips

At the end of each wing, air escapes from the high-pressure region at the bottom of the wing to the low-pressure region at the top of the wing. This produces vortices at the tips which leads to induced drag. The wing tip shape affects the spacing of these vortices. A hoerner tip increases the distance between vortex points, while keeping the same span length. It is indeed the most ideal low-drag tip; however, it is difficult to manufacture. Instead, a simple flat tip was used.

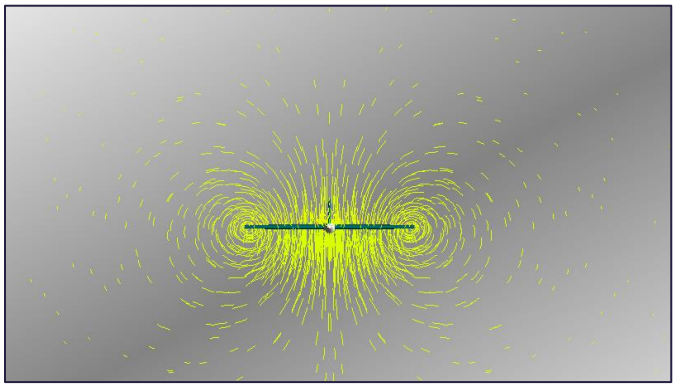

Figure 3: Vortices Around the Aircraft

4.2 Fuselage

A cross-sectional view of the team's fuselage shown in Figure 4 illustrates how it facilitates manufacturing and access to various chambers, while maintaining an aerodynamical shape. The fuselage is made of 13 rings of variable size that is defined by taper of the fuselage. The rings are held together by walls. The rings, plates and other components interlock with each other like puzzle pieces. A length of the 93.5 *in* was chosen, which approximately 70% of the wingspan is. The upper portion of the fuselage is flat. The fuselage has a cap that comes off, allowing placement of passengers, luggage and other electronics.

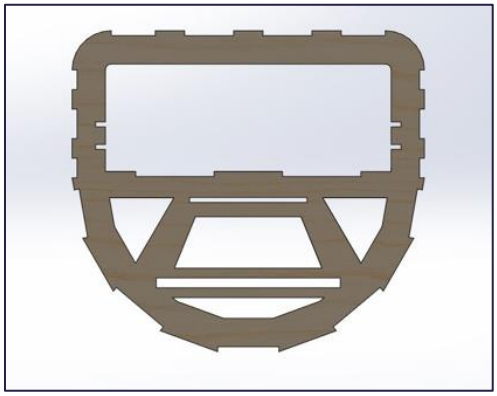

Figure 4: Cross Section View

4.3 Tail

The purpose of a tail is to counter the moments produced by the wing. The tail effectiveness is directly proportional to the lift produced by the tail and length of the tail moment arm from the center of gravity. During sizing, 65 *in* moment arm was used. A conventional tail arrangement was chosen because of its structural simplicity.

4.3.1 Horizontal Stabilizer

The horizontal stabilizer must counter pitching moments. It must be designed so that it must stall after the wings at any point during flight. The horizontal tail was set in line with the wings. The horizontal

tail has a negative incidence angle of 2 ° to trim the wing pitching moment. NACA 0013 airfoil was selected for the horizontal stabilizer. This is a symmetrical airfoil which provides both positive and negative lift throughout flight if needed. The horizontal stabilizer was sized using Raymer's Tail volume coefficient method. The horizontal tail volume coefficient was assumed to be 0.7. The reference area was then found to be 756 in^2. With the aspect ratio of 4, the span was calculated to be 55 *in.* A taper ratio of 0.6 was chosen. The corresponding root and tip airfoil chord length becomes 17.2 *in* and 10.3 *in.*

4.3.2 Vertical stabilizer

The vertical stabilizer must counter yawing moments, which are most directly related to the wing mean chord. Symmetric NACA 0015 airfoil was selected to have equal yaw in both directions. The thickness ratio of this airfoil is same as that of the wings. The vertical stabilizer was also sized using Raymer's method. A volume coefficient of 0.04 was used. The vertical stabilizer is mounted directly above the horizontal stabilizer. Hence, the moment length becomes 65 *in*. Thus, the area was calculated to be 273 in^2. An aspect ratio of 1.5 was selected and the taper ratio was same as that of horizontal stabilizer. Hence, the height becomes 20.2 *in*. The root and tip chord lengths were found to be 16.9 *in* and 10.1 *in*.

4.4 Control Surface Sizing

The control surfaces were sized according guidelines provided by Raymer. Ailerons are typically 15-25% of the wing chord, located outward toward the tips to produce the greatest moment about the longitudinal axis. The ailerons for this aircraft span the entire outward tapered region with a constant chord length of 5 *in*. While ailerons at the outward 10% length of the wing provide little control effectiveness due to tip vortices, it was decided to extend them all the way out for aesthetic purposes.

Rudders and elevators are typically 25-50% of the tail chord. The elevators of the aircraft have 4.5 *in* chord and span the whole length of the horizontal surfaces. Two servo motors were used in elevators to minimize the flutter. The rudder spans the entire height of the horizontal stabilizer, with a constant chord of 4.5 *in* that extends into a notched aerodynamic balance towards the top. An aerodynamic balance is an

optimized control surface geometry that extends in front of the hinge line. It is used to lessen the force required to deflect the surface and to reduce flutter tendencies.

With the servo and push rod configuration, the ailerons can deflect 25° up and 15° down. The elevators can deflect 20° up, and 15° down, while the rudder deflects up to 25° on either side.

4.5 Landing Gear

4.5.1 Configuration Selection

The positioning and design of the landing gear was determined comparing two most common configurations; the tail dragger and tricycle arrangement. Where a taildragger has two main wheels slightly forward of the aircraft's center of gravity, and a steerable tailwheel attached to the plane's rudder, a tricycle has a forward nose wheel used for steering, and two rear wheels. The image below shows both configurations for better understanding.

Figure 5: Landing Gear Configurations

The taildragger arrangement was chosen over the tricycle arrangement because it provides greater propeller clearance, reduced parasitic drag, an increased AoA during takeoff. Thus reducing take off velocity. The trade-offs display a greater difficulty with takeoff, landing and ground steering compared to a tricycle setup.

4.5.2 Layout Design and Wheel Size

In order to implement this design on the team's plane, the focus was concentrated on addressing issues that most commonly result from a tailwheel configuration. To prevent the aircraft from overturning, the main wheels were placed laterally and separately beyond a 25° angle off the center of gravity. This detail is important in the event that the center of gravity is too far behind the main wheels, the aircraft will ground loop. Similarly, if it is too forward, it may nose over. The tail down angle was designed to be about 15° with the gear in its static position.

To determine what size the wheels should be, maximum weight of the aircraft was first estimated to be 50 *lb*. The team decided that the aft tires should be about a quarter to a third of the size of the main wheels. The table below was used to select main wheels. The diameter of main wheel chosen is 4.5 *in* with 1.47 *in* width, and diameter of tailwheel is 1.67 *in* and 1 *in* width. From a simple static analysis, it is estimated that the front wheels are take about 42 *lb*, or 83% of the total weight at rest.

Table 2: Wheel Appropriate Widths and Diameters

Main wheels diameter or width (in.) = $A\ W_W^B$	Diameter		Width	
	A	B	A	B
General aviation	1.51	0.349	0.7150	0.312
Business twin	2.69	0.251	1.170	0.216
Transport/bomber	1.63	0.315	0.1043	0.480
Jet fighter/trainer	1.59	0.302	0.0980	0.467

W_W = Weight on Wheel

5. ELECTRONICS

5.1 Battery

A Turnigy Graphene 6S 6000 *mAh* lithium polymer battery with a 65C rating was chosen in accordance with competition rules. The 65C rating ensures a safe continuous discharge well above the required 45 *A* during flight with the power limiter installed. It also ensures that the battery will stay cool throughout operation. The battery is able to operate at maximum voltage for a long time. The 2.5 *lb* weight of the battery also makes it a good ballast item.

Following the general guideline of not allowing a LiPo to discharge beyond 75-80% of its full capacity, roughly 4500 *mAh* of charge can be provided during flight without damaging the battery and thus ensuring much reusability. The minimum flight time was calculated to be 6 *min*.

5.2 Speed Controller and Wiring

A Castle Talon Electronic Speed Controller (ESC) rated at 90 *A* is used to control the motor. It includes a built in heavy duty Battery Eliminator Circuit (BEC) that provides 6 *V* to the receiver and servo motors. XT90 connectors, rated for 90 *A* constant current, were soldered between wires to match the connector that came attached to the battery. A 12-gauge wire is used to match the gauge of the motor and ESC wires and to easily fit inside the connectors. The weakest current handling connections are at the

power limiter, which uses an XT60 connector rated for 60 *A*, and at the red arming plug, which uses a Deans ultra-plug rated between 50 *A* and 60 *A*. All the value are above maximum current to be encountered during flight. This ensures that there will be no overheating.

5.3 Servos

A Hitec HS-645MG analog servo was selected to drive each control surface. It can deliver 8.31 *lb-in* of torque at 6 *V* input. Five servos are used in total, one for each control surface (two ailerons, two elevators and a rudder). To verify that the servo is adequately capable of moving each surface, the torque was approximated as needed to move an aileron with the very conservative assumption that the expected freestream dynamic pressure acts evenly over its entire area and generates a vertical net force on its center.

5.4 Radio System

A Spektrum 2.4 *GHz* DX6e transmitter is paired with a Spektrum AR610 receiver. This setup allows for six channels, all of which are occupied (one throttle and five servos).

6. POWER AND PROPULSION

6.1 Motor

A motor was selected on the merits of high torque, 6S lithium polymer voltage range compatibility, and high-power rating. An E-flite Power 90 brushless electric motor was selected. It has 325 KV rating, making it capable of spinning at 8190 *RPM* under no load. It can continuously take 50 *A* of current or up to 1800 *W* of power. A motor with a lower KV provide more torque than a higher KV motor at the same power rating, thereby rotating a larger propeller.

During testing, it was found that with the chosen propeller, the motor overheats and begins to sporadically cut power after about two minutes at full throttle. This was for a static thrust test, and so the tendency to overheat is thought to greatly diminish as the motor is cooled by the additional free stream air during flight.

6.2 Propeller

The propeller is a twisted spinning airfoil that generates the thrust to move the aircraft forward. A propeller of high diameter and low pitch is ideal for a relatively low speed and high weight arrangement. It aids in quickly generating the necessary thrust for takeoff, somewhat akin to a car better able to climb a hill at low gear. After testing 20 propellers of various diameter, pitch, and shape, the Aerostar 19x6 Gas Series wood propeller was chosen for the reasons discussed below.

6.3 Thrust

Since the thrust produced by a propeller is a complex function of its geometry and must typically be experimentally derived, a thrust stand, shown in Figure 6, was built to test different propellers with the combination of motor, ESC, and battery. The working principle is that if moment arms from the axis of rotation are equal, the thrust produced by the propeller is registered as a weight by the scale. A Watt meter was used to measure the power supplied to the motor from the battery and to ensure it does not exceed the 1000 *W* limit. The Propeller capable of producing the highest thrust at the lowest power was chosen for flight. The upper size range of propellers tested was slightly above what was recommended by the motor manufacturer. Table 3 below displays the results of the experiment.

Figure 6: Thrust Stand

Table 3: Propeller Testing Data

Model	Diameter (*in*)	Pitch (*in*)	Max Power (*W*)	Max Thrust (*lb*)	Thrust Efficiency (*W/lb*)
Master Airscrew K Series	14	6	340	4.4	77.3
TGS Precision Sport	14	7	330	3.9	84.6
Aerostar Electric Series Wood	14	7	400	4.3	93
TGS Precision Sport	14	8	520	4.9	106.1
Turnigy	15	4.5	420	5.5	76.4
Master Airscrew K Series	15	6	430	5.5	78.2
TGS Precision Sport	15	8	500	6	83.3
Master Airscrew	16	6	680	7.7	88.3
Master Airscrew K Series	16	8	780	8.5	91.8
Master Airscrew 3 Blades	16	8	980	10	98
JFX	16	8	740	8.1	91.4

Aerostar Gas Series Wood	16	8	800	8.5	94.1
Aerostar Electric Series Wood	17	6	740	8.5	87.1
Turnigy Cherry Wood	17	8	940	10	94
TGS Precision Sport	17	8	700	8.4	83.3
Turnigy 3D Gas	17	8	990	9.5	104.2
Aerostar Electric Series Wood	18	8	970	10	97
TGS Precision Sport	18	8	810	9.4	86.2
Aerostar Gas Series Wood	19	6	990	11.2	88.4
Turnigy Gas Series Wood	19	8	980	10.8	90.7

Table 4: Aerostar Gas Series Propeller Data

Current (*A*)	4.3	8.3	13.3	17	21.3	27	30	35.8	39	44
Power (*W*)	100	200	300	400	500	600	700	800	900	980
Thrust (*lb*)	2.1	3.6	5	6	6.9	8	8.7	9.6	10.3	10.8
W/lb	47.6	55.6	60	66.7	72.5	75	80.5	83.3	87.4	90.7

This chosen propeller was then tested more extensively across different throttle settings. Table 4 shows that as input power increases, the power necessary to produce a pound of thrust increases so the propulsion system become less efficient. For a discharged battery, the maximum static thrust produced drops from just over 11 *lb* to between 9.5-10 *lb*.

During flight, thrust will decrease as velocity increases. Taking the more negative slope from the plot of measured data from previous SAE teams, as indicated in Nichol's white paper, the dynamic thrust is estimated as a function of velocity, as follows: $T_{dynamic} = 11 - 0.066V$.

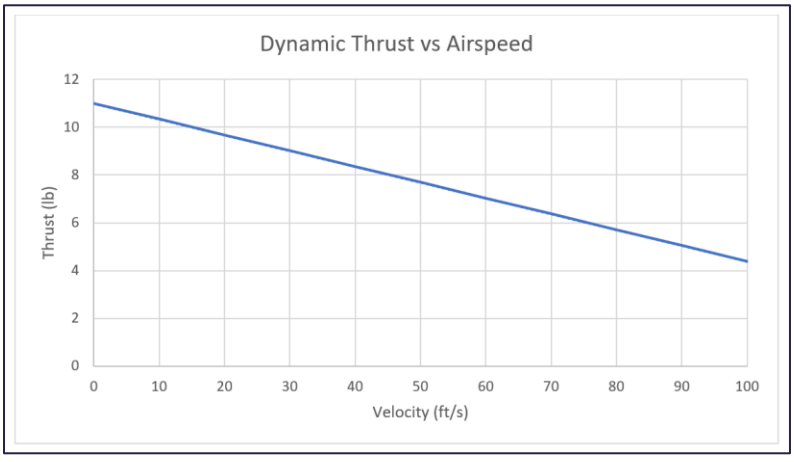

Figure 7: Thrust vs. Velocity Graph

7. LOADS

During cruise, the only forces acting on the aircraft are lift, drag, weight and thrust. Under any circumstances, the lift of the aircraft must be equal to total weight of the aircraft at that time. Almost all of the lift is generated by wings. Hence, the shaft that used to attach the wings to the fuselage must have high Young's Modulus to prevent any plastic damage by bending moment created by wings. Considering this effect, a wooden shaft of 1 *in* diameter was selected. The rear spar for the wings and the spars for tail section have 0.5 *in* diameter. Drag is a restrictive force originating from friction and viscous effects. During flight, the thrust must be greater than or equal to drag to keep aircraft moving. The thrust generated by the chosen propeller is sufficient to overcome drag. A special attention was paid towards reinforcing the plate the holds front landing gear because not it will support most of the weight of the aircraft, but it will also face high impulsive force during landing. This will also amplify the bearing stress at the location where screws are secured. Hence, to prevent fracture, 0.25 *in* thick birch plywood sheets was used secured on all sides by interlocking with fuselage frame to distribute the load.

8. FLIGHT ANALYSIS AND AIRCRAFT PERFORMANCE

8.1 Lift and Drag Analysis

The pressure and shear stress acting on aircraft result in lift and drag force. Accurately predicting drag force has been a challenge for aerodynamicists for centuries. Several techniques have been developed overtime to attempt to predict lift and drag force coefficients, which are lift and drag forces normalized with respect to dynamic pressure and wetted area respectively. The upcoming section discusses the combination of modern and historical methods to estimate lift and drag coefficients of the aircraft.

8.1.1 Lift on Airfoil and Wing

Several NACA airfoils were generated in MATLAB and imported into Fluent. The fluid domain was made 50 times bigger than the chord length. The area near the airfoil was very densely meshed. A K-Omega SST model for turbulence was elected to accurately predict drag on the airfoil. A Reynolds number of 400,000 was picked based on the assumption of cruise speed and chord length. Standard temperature and pressure of air was chosen. The parameters for the simulation are listed in Table 5. From CFD results,

it was clear that NACA 6415 and NACA 6412 have higher values of lift coefficients at different angles of attack. All the airfoils stall at between 14-16° AoA. The variation in drag coefficients was negligible at low AoA.

Table 5: Simulation Parameters

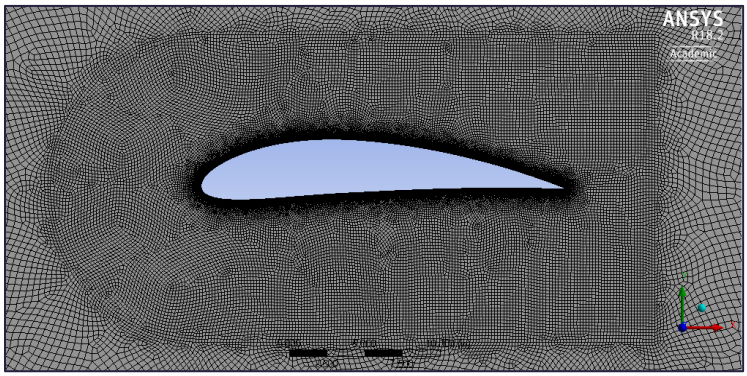

Parameter	Value
Temperature	$81\ °F$
Density	$2.375E^{-}3\ \frac{slug}{ft^3}$
Free Stream Velocity	$40\ \frac{ft}{s}$
Reynolds Number	400,000
Pressure	$0\ psig$

Figure 8: Mesh of the Airfoil

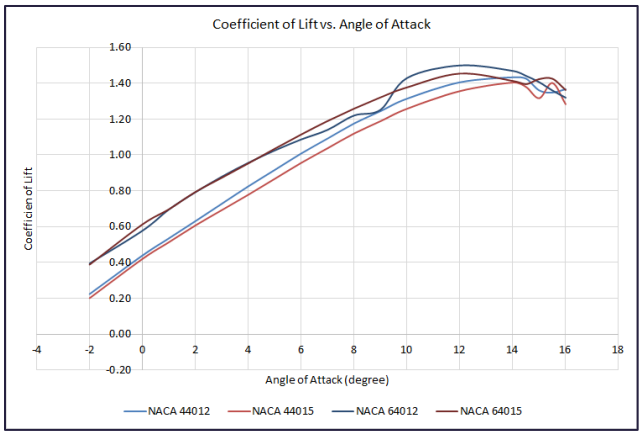

Figure 9: C_l vs. AoA for Airfoils

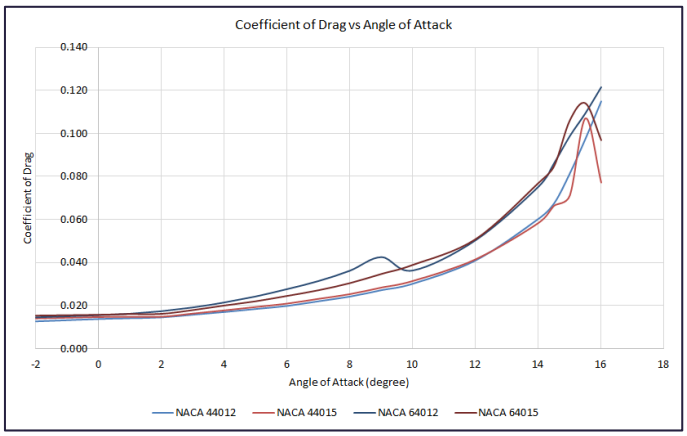

Figure 10: C_d vs. AoA for Airfoil

Using a linear fit for the NACA 6415 airfoil in the region where the airfoil does not stall, the value of slope was obtained. According to the CFD results,

$$C_{l_\alpha} = 5.53518\ rad^{-1} = 0.0966\ \deg^{-1}.$$

This represents a slope of 2D cross section and will be valid for a wing of infinite aspect ratio. Since this is a finite AR,

$$C_L = \left[\frac{dC_L}{d\alpha}\right] = \frac{5.53518(AR)}{2+[4+(AR)^2]^{\frac{1}{2}}} = 4.054\ rad^{-1} = 0.071\ \deg^{-1}.$$

It must be noted that the wings are tapered as well. Hence, it is expected to obtain a slightly better value for the slope of C_L than the one given above. A zero-lift angle of attack represents the AoA at which

no lift is produced. From experiments, the zero-lift AoA was calculated to be –5.8°. Therefore, the equation for C_L can be written as

$$C_L = 0.071\ (\alpha + 5.8)\ ^{(1)}$$

8.1.2 Drag Analysis

There are multiple sources of drag force. In general, drag can be classified as fixed drag and induced drag. The fixed drag arises from the pressure and shear forces acting on the exposed (wetted) surface of the aircraft. Induced drag represents the drag due to lift. This induced drag can further be divided into inviscid and viscid drag. In the section below, the total drag on the aircraft is estimated.

Fixed Drag: This is also known as C_{DO}, arising from the wetted area of the aircraft. The reference area used for calculations was the planform area of the wing. Nichol's White paper provided by SAE provides a method to estimate the skin drag on various components of the aircraft. The table below contains the value of drag for each individual component. Hence, the C_{DO} for the team's aircraft is 0.02210

Table 6: Drag Coefficients Involved with Each Component

Component	Fuselage	Wing	Horizontal Tail	Vertical Tail	Motor	Landing Gear	**Total**
C_{DO}	0.00316	0.01	0.00125	0.0005	0.0005	0.0042	**0.0221**

Induced Drag: This is the drag induced due to the lift. It is also known as inviscid drag, arising due to vortices. It is parabolic in nature and a function of aspect ratio of the wing and planform shape. With AR and Oswald efficiency factor known, it can be estimated as

$$C_{D,ind} = KC_L^2 = \frac{C_L^2}{\pi(AR)e} = 0.05925\ C_L^2$$

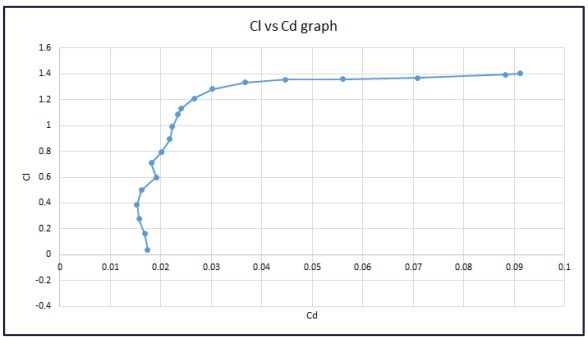

Figure 11: C_l vs C_d Graph of Airfoil

Viscous Drag: This is the drag term originating from the viscous forces acting on the wing. It depends upon the airfoil used. Let $C_{L,min}$ be the value of lift coefficient at the AoA that has lowest value of drag coefficient. Then, according to the convention, viscous drag is approximated as

$$C_{D,vis} = K_1(C_L - C_{L_{min}})^2 = 0.0142(C_L - 0.388)^2$$

Several other sources of drag were ignored because the flight will be in subsonic and incompressible region. The full drag equation turns out to be:

$$C_D = 0.0221 + 0.05925(C_L)^2 + 0.0142(C_L - 0.388)^2 \quad (2)$$

8.1.3 Full Model CFD Simulation

The assembly of the aircraft was created SolidWorks. Simulation parameters and turbulence model was kept same as that of airfoil. The following data for drag was obtained from the simulation.

Table 7: Drag Force on Each Component

Component	Fuselage	Wing	Tail	Rudder	Wingtip	Rudder Tip	Back	Front	**Total**
Drag (*lb*)	0.118	3.17	0.11	0.096	0.006	0.001	0.01	0.06	**3.71**

Following is the pie chart of lift and drag on the entire aircraft. As expected, the wings contribute towards most of the drag since lift-induced drag is dominant at low speeds.

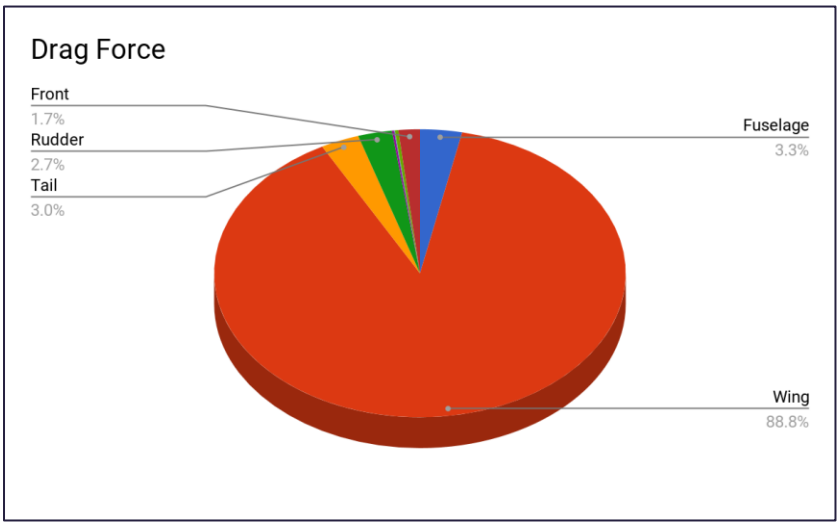

Figure 12: Pie Chart Showing drag on Each component

8.2 Ground Run and Takeoff

To estimate ground run distance, the team initially estimated the takeoff velocity. Friction was ignored during ground run, although it is present. According to the convention, take off velocity must be 1.2 times larger than the stall velocity. Stall velocity is the minimum velocity at which an aircraft must be flown in order to sustain flight. It also corresponds to velocity at highest value of the lift coefficient.

$$V_{LO} = \sqrt{\frac{2.88\,(\frac{W}{S})}{\rho C_{L_{max,TO}}}} = 51\ ft/s$$

Propeller efficiency represents how much torque is converted into thrust power by propeller. The team assumed a standard value of 0.85 for propeller efficiency. The maximum horsepower supplied is 1.334 HP. Under these circumstances, the takeoff distance becomes $d = \frac{V_{LO}^3}{1100\eta_p g\left(\frac{HP}{W}\right)} = 165ft.$

It must be noted that the horizontal stabilizer also contributes towards the lift. Hence, the team is expecting a smaller take off distance. It is also important to have an idea of the drag force while take off. Using a value of 1.1 for C_L, the C_D can be solved by using equation ***(2)*** to be 0.1. Hence drag force becomes 6.75 *lb*. Since the static thrust is 11 *lb* and dynamic thrust is 8 *lb*, the drag force during takeoff can be overcome easily.

8.3 Payload Prediction Curve

The amount of payload an aircraft can carry is an important consideration. For an electrical aircraft, the horsepower supplied by the motor stays constant. Hence, the lift force becomes a function of the density of the aircraft, which goes down with elevation. The lift at given elevation becomes $L = \frac{\rho}{\rho_{SL}} L_{SL}$. The payload fraction (PF) represents the ratio of the payload to the total weight of the aircraft, as shown here $PF = 1 - \frac{W_{empty}}{Wtot}$. The density of air at a given elevation can be found using the formula below, where P and T is pressure and temperature at given altitude: $\rho = \frac{P}{(1718(T+459.7))}$

Density altitude is defined as an altitude relative to the standard atmosphere conditions (ISA) at which the air density would be equal to the indicated air density at the place of observation. It is given by the formula below, where DA is density altitude, T_{SL} is standard atmospheric temperature, Γ is the slope of temperature versus elevation curve (0.00356 *F/ ft*), R is the universal gas constant, g is earth's gravity and M is the molecular mass of the air:

$$DA = \frac{T_{SL}}{\Gamma}\left[1 - \left(\frac{\frac{P}{P_{SL}}}{\frac{T}{T_{SL}}}\right)^{\frac{\Gamma R}{gM - \Gamma R}}\right]$$

The graph for payload fraction versus density altitude, also known as the payload prediction curve, is shown below.

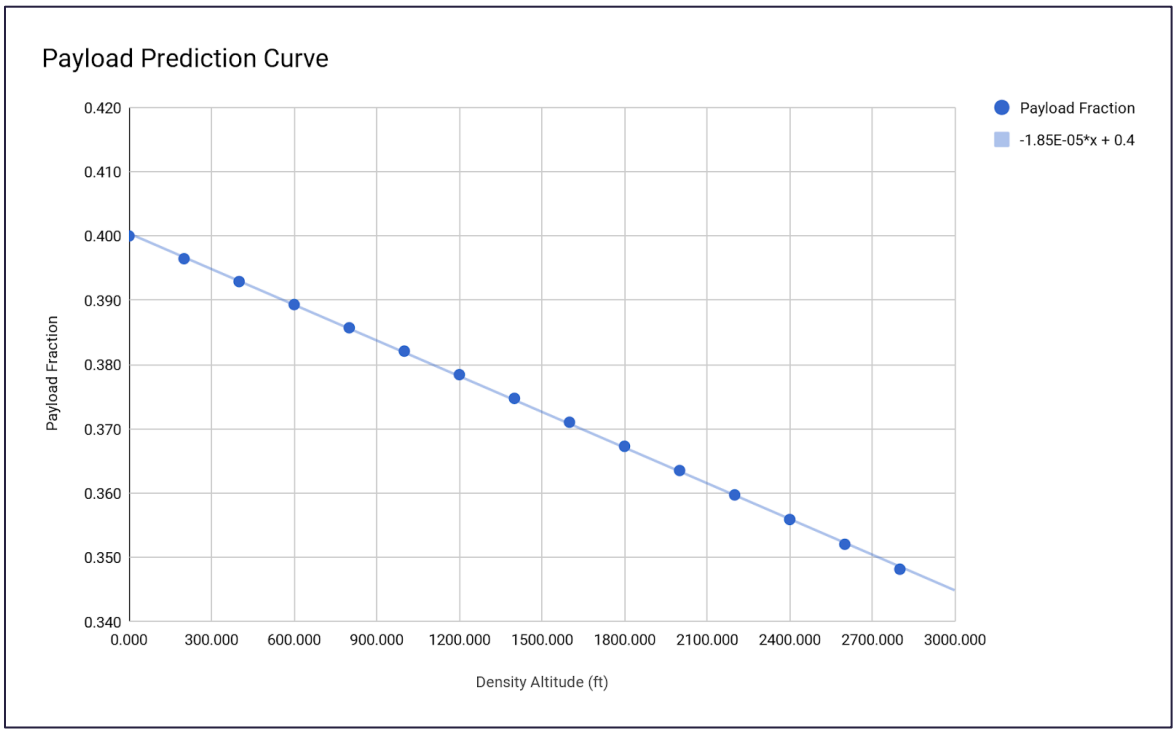

Figure 13: Payload Prediction Curve

9. STABILITY AND CONTROL

9.1 Static Stability

Stability requires an aircraft to restore itself to its equilibrium position after a disturbance. Where Static stability is concerned with the aircraft's behavior immediately after a disturbance, dynamic stability is a transient response to both a disturbance and an input command. An aircraft must be statically stable to become dynamically stable, which may not always be the case.

Longitudinal stability is the most important direction to evaluate since it is necessary for level flight. An aircraft is in equilibrium about its lateral axis if its net pitching moment is 0. The neutral point, or aft limit is the center of gravity location where the aircraft is neutral, in other words $\frac{dC_m}{dC_l} = 0$. Therefore,

the criterion for longitudinal static stability is a center of gravity location such that $\frac{dC_m}{dC_l} < 0$, such the center of gravity lies in front of the neutral point.

The pitching moment is taken with respect to the aerodynamic center (AC) of the wing. This is the point at which the moment does not change with angle of attack. For the chosen airfoil, AC was found to be at 25 % of MAC behind the leading edge of the wing. The variation of coefficient of moment with C_L is as follows:

$$\frac{dC_M}{dC_L} = \left(\frac{x_{cg}}{\bar{c}} - \frac{x_{ac}}{\bar{c}}\right) - \left(\frac{a_t}{a_w}\right)(\eta_t)(c_{HT})\left(1 - \frac{d\varepsilon}{d_{\alpha_w}}\right) = 0$$

The first term represents the stability contribution of the center of gravity with respect to the AC of the wing and the second term displays the contribution of the tail. The distances are normalized with MAC. a_t and a_w are the slopes of the tail and wing's coefficient of lift respectively. approximated using the following equations: $a_t = \frac{dC_L}{d\alpha} = \frac{5.7684\ (AR)}{1+\sqrt{\left[1+\left(\frac{AR}{2cos\Lambda}\right)^2\right]}} = 3.56$ and $a_w = \frac{dC_L}{d\alpha} = 4.054$ η_t is the tail efficiency, assumed to be 0.8. Horizontal tail volume coefficient of 0.67 as mentioned above. $\frac{dE}{da}$ is the change in downwash angle with respect to the AoA. A typical value is 0.33. Plugging all the values in to find the location of the neutral point:

$$\left(\frac{x_{cg}}{22.55} - 0.25\right) - \left(\frac{3.56}{4.054}\right)(0.8)(0.67)(1 - 0.33) = 0, \text{ hence: } x_{cg} = N_0 = 12.75\ in$$

The neutral point is thus calculated to be 12.75 *in* (57% of MAC) from the leading edge of the wing.

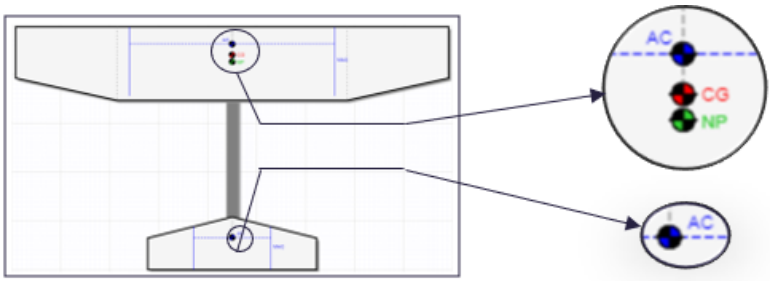

Figure 14: Pictorial Representation of Various Points

The static margin (SM) is the allowable distance from the neutral point to the center of gravity. Here it is assumed to be at a standard positive value of 10% of the MAC, so that *SM*=2.3 *in*. The design c_g location is hence 10.5 *in* from the wing leading edge. The neutral point value was checked against two different center of gravity calculators provided online. The average neutral point obtained

from these was found to be about 29.25 *in* from the front, making the design center of gravity about 27 *in* with the assumed static margin. These are more conservative values and so are to be used instead for a higher factor of safety when flying.

9.2 Mass Balancing

After manufacturing the fuselage and final assembly prior to the test flight, it was found that the plane was significantly tail heavy. To reach the neutral point in the unloaded configuration, the center of gravity had to be shifted 5 *in* forward. With 12 *lb* of removable ballast weight placed 18 *in* from the front, the aircraft can operate just forward of its conservative neutral point during flight at an unloaded weight of 39 *lb* and operate at the design Cg with a ballast of 5 *lb* at a total loaded weight of 51 *lb*.

10. MANUFACTURING

The fabrication of the aircraft was divided into different sections: the wings and empennage, the fuselage, the wiring and the landing gear. All sections were assembled in the end.

10.1 Wings and Empennage

The wings and empennage are made of EPP foam core. The foam cores were covered with 0.06 *in* balsa wood sheets to increase strength and finally covered with Monokote film. Below is the procedure:

1. Foam cores were shaped according to the airfoils using a hot wire device
2. 0.06 *in* balsa wood sheets were soaked in water for improved malleability
3. Soaked balsa wood sheets were shaped to bend around the leading edge of the wings
4. Wood glue was used to adhere the balsa wood sheets to the wings' leading edge
5. Entire wing was coated with similar balsa wood sheets using adhesive spray
6. The balsa wood sheets were sanded to create a smooth surface and slots were cut for wiring
7. Monokote was applied using a hot iron tool and a heat gun
8. Flat nylon hinges were used to connect the control surfaces to the wings
9. Control horns were installed on the control surfaces and attached to the servos using push rods

10.2 Fuselage

Most of the fuselage is made with 0.13 *in* thick birch plywood. Various components of fuselage interlock with themselves as puzzle pieces. The following procedure was used fabricate the frame:

1. 0.13 *in* birch plywood was laser cut based on CAD drawings
2. Mating edges were sanded for a smooth connection and were glued together using wood glue
3. The surfaces were temporarily held together using rubber bands and strings while the glue cured
4. Monokote was applied using a hot iron tool and a heat gun

The fuselage has three compartments with sub-compartments. The middle compartment contains two sections, the passengers bay and the luggage bay (cargo). The passengers were placed into laser-cut wooden slots, fitting three tennis balls in each row. The last tennis ball plate holds 2 passengers per row. The cargo bay is in front of the passenger compartment.

Ten 16-gauge 0.06 *in* steel metal sheets of 18 x 6 *in* size were purchased and used for the luggage. The metal sheets were cut into thirds to create 6 x 6 *in* square sheets, generating a total of 30 sheets. The edges were sanded to ensure smooth contact between each plate while stacking and prevent any injury by sharp cuts. Two 0.5 *in* diameter holes were drilled four inches apart, roughly one inch from two opposing corners for each plate. Two 1.25 *in* bolts are used to secure the luggage together with a washer and a nut. Each steel metal sheet weighs 0.55 *lb*.

10.3 Electronics

The electronics wiring is installed using the following procedure:

1. From the nose, wires run from the motor to the ESC reaching to the battery
2. The battery is wired to the receiver, the power limiter and the red arming plug
3. The servo extensions branched off to the five servo motors used
4. The servo motors were secured to their respective notches with CA glue. The extension cables were also glued together to ensure they do not disconnect during flight

10.4 Landing Gear

The front landing gear frame is made of aluminum with two 4.5 *in* diameter rubber wheels. The landing gear was screwed into 0.25 *in* thick sheet of birch plywood, located 2 *in* below the cargo

compartment. Two 2 *in* long fully threaded 0.5 *in* diameter bolts were used to secure the front landing gear. The rear landing gear is made up of steel with a 1.75 *in* diameter rubber wheel. Based on this landing gear configuration, the AoA is 10°.

10.5 Assembly

The fuselage's assembly was split into the following subassemblies: front, middle and aft section. Separating the assembly process into these three sections allowed us to work meticulously on each subassembly, while placing great attention to detail. The passenger and cargo bays were assembled first. A greater detail was paid the front and aft section because of tapering.

Figure 15: Subassemblies of Fuselage

The entire assembly was put together with laser cut rings and walls that were secured with wood glue. First, one side of the framework of the passenger and cargo bay was assembled. Rings were then inserted and secured at the opposite end, locking them in place. Additional patches and hooks were added to provide reinforce any weak corners. A full day of drying time was provided before starting the next subassembly. The steps were repeated for the forward and aft section except both sub-assemblies were put together upside down, to protect the taper that occurs on the sides and bottom of the fuselage.

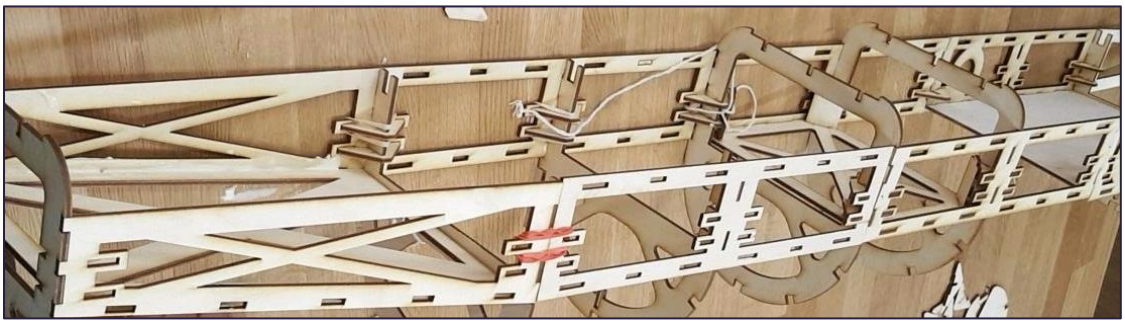

Figure 16: Middle section of Fuselage

Once the fuselage was assembled, the horizontal and vertical stabilizers were glued in using wood glue. The spars were used to prevent their dislocation. The wings were kept detachable to facilitate shipping and handling.

10.6 Test Integration

Prior to initiating the final assembly process, it was paramount to first create a prototype of the team's fuselage framework. This would allow to test what parts of the fuselage needed to be reinforced or reconsidered after conducting a drop test. Due to funding and cost constraints, the fuselage was prototyped to be one third of the size of the actual fuselage.

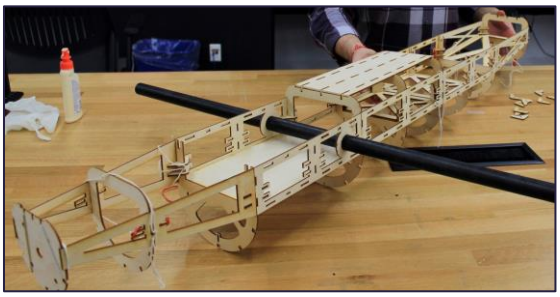

Figure 17: Fuselage Prototype

Upon completing this prototype's assembly, it was put through a drop test at a height of six feet off the ground. As a result, a few rings snapped, and some areas of the framework were dismantled. This drop test corroborated that parts of the fuselage needed to be reinforced in particularly weak areas of connection.

Figure 18: Fractured Rings of Fuselage

A number of steps were taken afterwards to strengthen the fuselage framework. They include the double layering of birch plywood used in rings that are subject to supporting majority of the load such as rings supporting cargo bay, addition of wider struts of wood that run along the length of the fuselage and using hooks and supports to areas that experienced breakage.

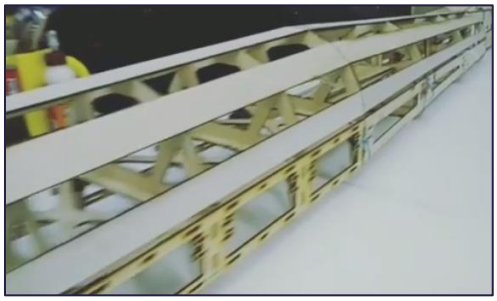

Figure 19: Strut Implementation

11. CONCLUSION

Team WingingIt successfully completed the design, manufacturing and testing phases of the SAE Aero Design Competition. The plane was designed to optimize the following three criteria: payload, maximum power and takeoff distance. Based on the rules of the competition, several guidelines and limitations were to be accounted for.

The shape of the fuselage was critical to maximize the carried payload, however limited the total weight. The fuselage is 93.5 *in* long and 9 *in* wide up to the tapered tail. It has 13 rings connected by

rods to ensure additional strength. The cross section was designed to trade-off between the benefits of the most aerodynamic shape (circular) and ease of manufacturing (rectangular). To compensate for the weight of the plane, the wings were designed to be almost the largest possible (within the size constraints) for maximum lift. The wing area, start of taper, and wingspan simultaneously created a high aspect ratio, hence a high coefficient of lift, notably on the wing. In addition, the wing airfoil is ideal to limit the drag force applied to the plane, and after several simulations, the NACA 6415 airfoil was chosen.

Maximum thrust is produced at the maximum allowable power provided to the motor, which is required for a high takeoff velocity and low takeoff distance. A vital component of the plane's design lay in the use of electronics. The goal was to generate the high torque for a large propeller and so an E-flite Power 90 brushless electric motor was chosen. This was coupled with an Aerostar 19 x 6 Gas Series wood propeller after testing a multitude of brands and sizes. A high capacity 6000mAh battery with a high discharge current rating was chosen as the power supply. All things considered, the propulsion system generated 11 *lb* of static thrust, sufficient enough to allow the plane to take off and maintain enough power to compensate the induced drag.

The wings and fuselage were designed to optimize the amount of payload carried with the maximum thrust produced under 1000 *W* of power. Therefore, the largest plane possible within the specific limitations was chosen for the design. The full payload (cargo and passengers) is 19 *lb* with a ballast of 5 *lb*, making for a total of 51 *lb*. The fuselage fits ten rows of three tennis balls each, totaling 30 passengers. With these parameters and successful flight rounds, the intended design flight score for the competition is 93.75.

12. REFERENCES

(1) Raymer, Daniel P. *Aircraft Design: a Conceptual Approach*. American Institute of Aeronautics and Astronautics, 2012.

(2) Hale, Francis J. *Introduction to Aircraft Performance, Selection, and Design*. John Wiley, 1984.

(3) “Airfoil Database Search (NACA 4 Digit).” *NACA 4 Digit Airfoil Database Search*, airfoiltools.com/search/index?m%5Bgrp%5D=naca4d&m%5Bsort%5D=1.

(4) “Density Altitude.” *Wikipedia*, en.wikipedia.org/wiki/Density_altitude.

(5) Anderson, John D. *Fundamentals of Aerodynamics*. McGraw-Hill Education, 2017.

(6) Benson, Tom. “Earth Atmosphere Model - English Units.” *NASA*, 12 June 2014, www.grc.nasa.gov/www/k-12/rocket/atmos.html.

(7) Budynas, Richard G. *Shigley´s Mechanical Engineering Design*. McGrae Hill, 2016.

(8) *Fluent - Flow over a 2-D Airfoil*, www.mne.psu.edu/cimbala/Learning/Fluent/fluent_airfoil.htm.

(9) RC Center of Gravity Calculator. https://rcplanes.online/cg_calc.htm

(10) ECalc Center of Gravity Calculator. https://www.ecalc.ch/cgcalc.php

(11) Hurt, Hugh Harrison. *Aerodynamics for Naval Aviators*. Aviation Supplies Et Academics, 2015.

APPENDIX A – TABLES OF ACRONYMS, UNITS, FIGURES AND TABLES

List of Acronyms		List of Physical Units	
Aerodynamic Center	AC	Acceleration	ft/s^2
Angle of Attack	AoA	Current	*A*
Aspect Ratio	AR	Density	$slug/ft^3$
Chord Length	c	Energy	*BTU*
Coefficient of Drag	C_d	Velocity	*ft/s*
Coefficient of Lift	C_l	Length	*ft*
Coefficient of Moment	C_m	Mass	*Slug*
Computation Fluid Dynamics	CFD	Power	*W*
Computer Aided Design	CAD	Pressure	*psi*
Density Altitude	DA	Resistance	*ohm*
Finite Element Analysis	FEA	Stress	*psi*
Mean Aerodynamical Chord	MAC	Temperature	*°F*
Pressure Altitude	PA	Thrust	*lb-in*
Reynolds Number	Re	Time	*s*
Sea Level	SL	Torque	*lb-in*
Sweep Angle	λ	Voltage	*V*

Table of Figures:

Figure 1: Design Process Flowchart 4
Figure 2: Pressure Distribution Over the Wing 5
Figure 3: Vortices Around the Aircraft 6
Figure 4: Cross Section View 6
Figure 5: Landing Gear Configurations 8
Figure 6: Thrust Stand 11
Figure 7: Thrust vs. Velocity graph 12
Figure 8: Mesh of the Airfoil 14
Figure 9: C_l vs. AoA for Airfoils 14
Figure 10: C_d vs. AoA for Airfoil 14
Figure 11: C_l vs C_d Graph of Airfoil 15
Figure 12: Pie Chart Showing Drag on Each component 16
Figure 13: Payload Prediction Curve 18
Figure 14: Pictorial Representation of Various Points 19
Figure 15: Subassemblies of Fuselage 22
Figure 16: Middle Section of Fuselage 22
Figure 17: Fuselage Prototype 23
Figure 18: Fractured Rings of Fuselage 23
Figure 19: Strut Implementation 23

Table of Tables:

Table 1: Schedule of Major Deliverables 3
Table 2: Wheel Appropriate Widths and Diameters 9
Table 3: Propeller Testing Data 11
Table 4: Aerostar Gas Series Propeller Data 12
Table 5: Simulation Parameters 14
Table 6: Drag Coefficients Involved with Each Component 15

APPENDIX B – TECHNICAL DATA SHEET: PAYLOAD PREDICTION

Elevation (ft)	Temperature ($°F$)	Pressure ($\frac{lb}{ft^2}$)	Density ($\frac{slug}{ft^3}$)	Density Altitude (ft)	Lift (lb)	Payload (lb)	Payload Fraction
0	59.00	2116.22	0.002377	0.00	45.00	18.00	0.400
200	58.29	2100.95	0.002363	200.07	44.74	17.74	0.396
400	57.57	2085.78	0.002349	400.15	44.47	17.47	0.393
600	56.86	2070.69	0.002335	600.22	44.21	17.21	0.389
800	56.15	2055.69	0.002322	800.29	43.95	16.95	0.386
1000	55.43	2040.78	0.002308	1000.37	43.70	16.70	0.382
1200	54.72	2025.96	0.002294	1200.44	43.44	16.44	0.378
1400	54.01	2011.22	0.002281	1400.51	43.18	16.18	0.375
1600	53.29	1996.57	0.002267	1600.59	42.93	15.93	0.371
1800	52.58	1982.01	0.002254	1800.66	42.67	15.67	0.367
2000	51.87	1967.53	0.002241	2000.73	42.42	15.42	0.364
2200	51.15	1953.14	0.002227	2200.80	42.17	15.17	0.360
2400	50.44	1938.83	0.002214	2400.88	41.92	14.92	0.356
2600	49.73	1924.61	0.002201	2600.95	41.67	14.67	0.352
2800	49.01	1910.48	0.002188	2801.02	41.42	14.42	0.348
3000	48.30	1896.43	0.002175	3001.09	41.18	14.18	0.344

APPENDIX C – 2D DRAWING